Quaternary Science Reviews 27 (2008) 1166–1180

Contents lists available at ScienceDirect

Quaternary Science Reviews

journal homepage: www.elsevier.com/locate/quascirev

Holocene changes in eastern tropical Pacific climate inferred from a Galápagos lake sediment record

Jessica L. Conroy [a,*], Jonathan T. Overpeck [a,b,c], Julia E. Cole [a,c], Timothy M. Shanahan [d], Miriam Steinitz-Kannan [e]

[a] Department of Geosciences, The University of Arizona, 1040 E. 4th Street, Tucson, AZ 85721, USA
[b] Institute for the Study of Planet Earth, The University of Arizona, 715 N. Park Avenue, 2nd Floor, Tucson, AZ 85721, USA
[c] Department of Atmospheric Sciences, The University of Arizona, 1118 E. 4th Street, Tucson, AZ 85721, USA
[d] Woods Hole Oceanographic Institution, MS #4, Woods Hole, MA 02543, USA
[e] Department of Biological Sciences, Northern Kentucky University, Highland Heights, KY 41099, USA

ARTICLE INFO

Article history:
Received 15 November 2007
Received in revised form
11 February 2008
Accepted 19 February 2008

ABSTRACT

Paleoclimate records from the tropical Pacific suggest the early to mid-Holocene was a period of reduced El Niño/Southern Oscillation (ENSO) variability, with a transition to modern, increased ENSO frequency occurring some time in the last few thousand years. However, the nature and timing of this shift remains uncertain due to the discontinuous nature and/or coarse resolution of many ENSO proxies, as well as a lack of agreement between previously published records. A new, continuous, climate record from El Junco Crater Lake in the Galápagos Islands reveals several abrupt changes in lake level and precipitation through the Holocene. Hydroclimatic model simulations suggest that El Junco lake level responds sensitively to increases in precipitation associated with El Niño events, rising during wet El Niño events and falling during the intervening dry periods. Grain size data from El Junco sediment cores indicate past lake level variability, likely associated with changing seasonal precipitation and ENSO frequency. The grain size data suggest increased precipitation intensity prior to 9000±120 cal years BP, and after 4200±130 cal years BP, as well as a two-step increase in precipitation at 3200±160 and 2000±100 cal years BP. Maximum Holocene precipitation and inferred ENSO variability occurred between 2000±100 and 1500±70 cal years BP, during the same period that six other independent proxy records suggest higher ENSO frequency and longer, stronger El Niño events. Decreasing sediment carbon/nitrogen (C/N) ratios in El Junco sediments indicate rising lake levels from the early Holocene to present, corroborating the grain size data. The inferred increase in precipitation at 4200±130 cal years BP and at 2000±100 cal years BP coincides with decreasing Southwest Asian and East Asian Monsoon intensity, suggesting tropical Pacific climate and the Asian monsoon were interconnected systems at centennial to millennial timescales during the Holocene. A weakening trend in the Asian monsoon and the trend toward wetter conditions at El Junco also coincide with a trend toward cooler and drier conditions inferred from Cariaco Basin sediment proxies from the mid-Holocene to present, suggesting the migration of the Intertropical Convergence Zone (ITCZ) likely influenced hydrological changes in both the eastern tropical Pacific and the Asian Monsoon region during the Holocene.

1. Introduction

Records of past climate variability from across the tropical Pacific Ocean indicate that the frequency and intensity of ENSO have varied through the Holocene. Some of these proxies record changes in tropical Pacific sea surface temperature (SST), whereas others reveal changes in the frequency and intensity of individual El Niño events through time (e.g., Shulmeister and Lees, 1995; McCulloch et al., 1996; Gagan et al., 1998; Fontugne et al., 1999; Sandweiss et al., 2001; Tudhope et al., 2001; Andrus et al., 2002; Koutavas et al., 2002; Moy et al., 2002; Riedinger et al., 2002; Cole, 2003; Loubere et al., 2003; Stott et al., 2004; Carre et al., 2005; Rein et al., 2005; Lea et al., 2006). The majority of these records suggest that ENSO frequency was substantially reduced during the early to mid-Holocene, and increased in frequency sometime in the last few thousand years. However, many ENSO reconstructions lack either length, resolution, continuity, or location within the central ENSO region. These deficiencies are usually due to the

* Corresponding author. Tel.: +1 520 621 8025; fax: +1 520 621 2672.
E-mail addresses: jconroy@email.arizona.edu (J.L. Conroy), jto@u.arizona.edu (J.T. Overpeck), tshanahan@whoi.edu (T.M. Shanahan), kannan@nku.edu (M. Steinitz-Kannan).

0277-3791/$ - see front matter © 2008 Elsevier Ltd. All rights reserved.
doi:10.1016/j.quascirev.2008.02.015

nature of the proxy: ocean sediments are long, continuous and located in the tropical Pacific, but often lack resolution because of low sedimentation rates. Corals from the tropical Pacific provide exceptional temporal resolution (monthly to seasonal), but lack the length and continuity to reconstruct variations occurring over centuries to millennia. Oxygen isotope values from mollusks and otoliths found in faunal middens can reveal high-resolution SST changes, but these records are short, discontinuous, and interpretation may or may not reflect open ocean conditions (DeVries and Wells, 1990; DeVries et al., 1997). In contrast, lake sediments can provide continuous records extending over several millennia and typically have high temporal resolution (although usually lower than that needed to reconstruct individual ENSO events).

The Galápagos Islands, located in the eastern equatorial Pacific, are an ideal site for paleoclimatic reconstructions of ENSO (Colinvaux, 1984). Interannual variability in most aspects of Galápagos climate is dominated by ENSO, as many of the physical processes fundamental to ENSO are centered in this region. This study presents a high-resolution, continuous, 9200-year record of tropical Pacific climate variability based on grain size measurements and C/N ratios derived from El Junco Crater Lake in the highlands of San Cristobal Island, Galápagos. In the following sections, we introduce our field area, methodology, and the results of a lake modeling study. We then present our grain size and C/N results and discuss our findings in a broader context.

2. Regional setting

2.1. Study site

The Galápagos Islands are located on the equator, 1000 km west of South America (Fig. 1). San Cristobal, one of the larger Galápagos Islands (558 km^2), lies in the southeast of the archipelago (0.8°S, 89.3°W). The southwest summit of the island is a large volcano that approaches 700 m elevation. The crater holding the 6-m deep El Junco Lake lies 675 m above sea level near the southwest summit of San Cristobal, where stratocumulus clouds usually conceal the lake in a dense fog. El Junco is a circular (280 m diameter), closed-basin, freshwater lake with a small catchment area (~0.13 km^2), extending from the rim of the crater ~60 m down to the water (Colinvaux, 1968, 1969). One overflow channel (age unknown), incised into the crater rim, limits lake level to 6 m. Although a detailed record of overflow is not available, we do know that water overflowed through this channel during the strong El Niño event of 1997–1998 (M. Steinitz-Kannan, personal communication). No perennial streams flow into the crater, and sediment transport into the lake is likely due to material eroding from the sides of the crater. Aquatic macrophytes were present along the shores of El Junco in September 2004, although the water fern *Azolla microphylla*, present in 1966, was absent (Colinvaux, 1972). The local vegetation surrounding El Junco Lake includes species found within the Miconia and fern–sedge zones, such as the species *Miconia robinsoniana* and *Cyathea weatherbyana* (Wiggins and Porter, 1971; Colinvaux and Schofield, 1976a, b). *Rubus niveus*, or hill raspberry, is an introduced species also present along the shoreline of El Junco (McMullen, 1999).

2.2. Galápagos climatology

The descent of cold, dry air coupled with trade wind-induced upwelling and cold SST sustain the typically arid climate of the Galápagos (Colinvaux, 1984). The cold SST around the islands also creates a thermal inversion layer, where air near the surface is colder than air aloft. The inversion layer is reflected in the layer of stratocumulus clouds over the islands and surrounding ocean, including El Junco (Colinvaux, 1984). During an El Niño event, trade winds slacken, upwelling weakens, the shallow marine thermocline is replaced with a deeper mixed layer, and the atmospheric inversion layer disintegrates. This is reflected in an increase in mid-level convective clouds and a decrease in stratocumulus clouds. Precipitation also increases substantially in the islands; during very strong El Niño events, monthly precipitation in the Galápagos can be more than an order of magnitude greater than rainfall during non-El Niño months (Fig. 2) (Snell and Rea, 1999). Table 1 demonstrates the strong relationship between Galápagos climate data and four ENSO Indices: the Niño 1+2, Niño 3, Niño 3.4 and Multivariate ENSO Index (MEI) (Wolter and Timlin, 1998; Smith and Reynolds, 2004). The Niño 1+2, Niño 3, and Niño 3.4 Indices are based on SST anomalies in the tropical Pacific from 0–10°S, 90–80°W; 5°N–5°S, 150–90°W; and 5°N–5°S, 170–120°W, respectively. The MEI is a basin-wide index integrating tropical Pacific sea-level pressure, the zonal and meridional components of the surface wind, SST, surface air temperature, and total cloudiness (Wolter and Timlin, 1998). The Galápagos straddle the border between the Niño 1+2 and Niño 3 regions, and Galápagos climate variables are most strongly correlated with Niño 1+2 values (Table 1).

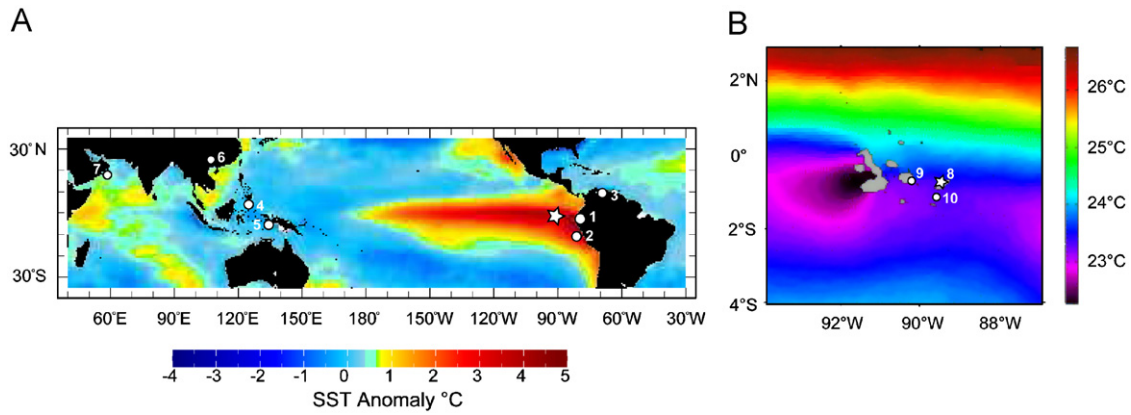

Fig. 1. (A) Map of tropical Pacific SST anomalies during the 1997/1998 El Niño event (Smith and Reynolds, 2004). Star indicates the location of the Galápagos Islands, circles indicate locations of paleoclimate proxy data plotted in Figs. 8 and 9. 1: Laguna Pallcacocha sediment record (Moy et al., 2002), 2: Peru Margin ocean lithic flux and SST records (Rein et al., 2005), 3: Cariaco Basin % Ti record (Haug et al., 2001), 4 and 5: Western tropical Pacific Ocean SST records (Stott et al., 2004), 6: $\delta^{18}O$ record from the Dongge Cave stalagmite (Yuan et al., 2004; Dykoski et al., 2005; Wang et al., 2005), 7: Oman Margin % *G. bulloides* record (Gupta et al., 2005). (B) Map of annual Galápagos SST modified from Palacios (2004), with 8: El Junco sediment record, 9: Bainbridge Crater Lake sediment record (Riedinger et al., 2002), and 10: Eastern tropical Pacific Ocean SST record (Koutavas et al., 2002).

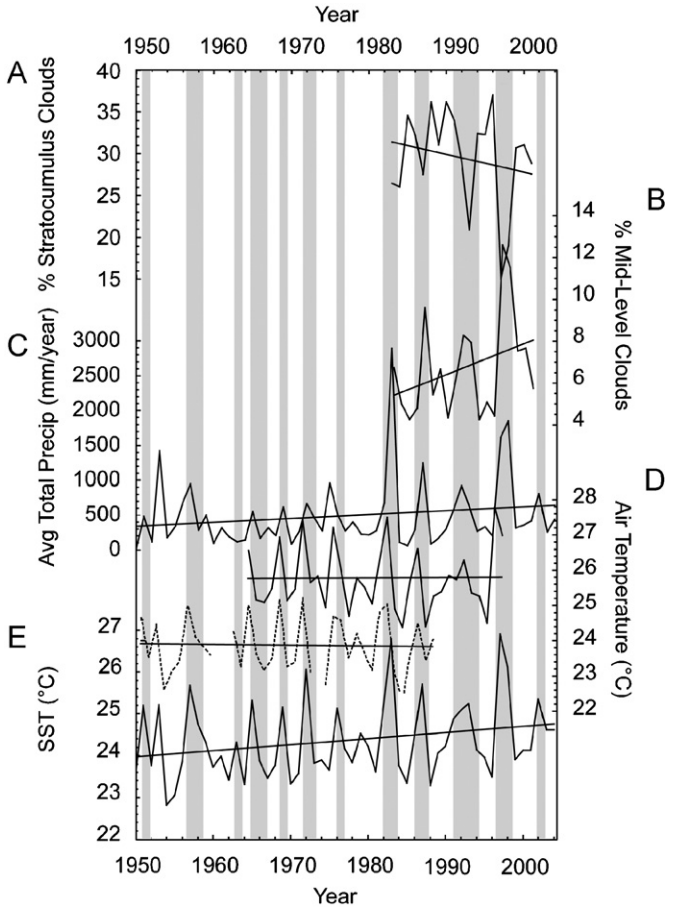

Fig. 2. Annual Galápagos climatic data. (A) International Cloud Climatology Project (ISCCP) percent stratocumulus clouds (Rossow et al., 1996). (B) ISCCP percent mid-level convective clouds (Rossow et al., 1996). (C) Total annual Galápagos precipitation (Snell and Rea, 1999). (D) Galápagos air temperatures: solid line is air temperature measured at Santa Cruz (Snell and Rea, 1999), and dashed line is air temperature measured at San Cristobal (Baker et al., 1994). (E) Galápagos SST (0–2°S, 88–90°W) (Smith and Reynolds, 2004). Linear trends are included on each time series. Gray bars represent El Niño events.

Table 1
Correlation coefficients for annual Galápagos SST, precipitation, air temperature, and clouds and the Niño 1+2, Niño 3, Niño 3.4 and Multivariate ENSO (MEI) indices, 1950–2004 (cloud data 1983–2001, air temperature 1950–1998)

	Niño 1+2	Niño 3	Niño 3.4	MEI
Galápagos SST	***0.98***	***0.92***	***0.76***	***0.81***
Galápagos precipitation	***0.78***	***0.60***	***0.41***	***0.54***
Galápagos air temperature[a]	***0.87***	***0.81***	***0.64***	***0.64***
Galápagos air temperature[b]	***0.86***	***0.87***	***0.79***	***0.73***
Stratocumulus clouds	***0.77***	***0.77***	0.52	***0.75***
Mid-level clouds	***−0.79***	***−0.64***	−0.42	***−0.56***

Significant correlation coefficients (95% confidence level, accounting for auto-correlation via effective sample size) are in bold.
[a] Santa Cruz air temperature.
[b] San Cristobal air temperature.

3. Methods

3.1. Field methods

We retrieved a 3.5 m core from the center of El Junco at a water depth of 6 m in September 2004 using a 9 cm diameter Nesje piston corer (Nesje, 1992). We also retrieved three mud–water interface cores (EJ-1, EJ-2, and EJ-3) that preserved the sediment–water boundary using a 7 cm diameter Aquatic Instruments gravity corer that was lowered gently into the sediment. The sediment–water interface in each of these three cores was preserved with minimal mixing. We subsampled the mud–water interface cores in the field at 0.5 cm intervals, as the sediment contained too much water to be transported intact. We used the Nesje core and one overlapping mud–water interface core (EJ-2), which is 46 cm long, in our study.

3.2. Age model

We created an age model for the cores using radiocarbon, ^{210}Pb, and ^{137}Cs measurements (Table 2). Measured ^{210}Pb and ^{137}Cs activities within the uppermost sediments of El Junco at 2 cm intervals are from a core taken in the center of the lake in 1991 (Steinitz-Kannan et al., 1998). We calculated ^{210}Pb ages based on these measurements, using the constant rate of supply model and ^{214}Bi as an equivalent of supported ^{210}Pb in the sediment (Krishnaswamy et al., 1971; Appleby and Oldfield, 1978; Appleby and Oldfield, 1983; Appleby, 2001). A ^{137}Cs bomb-spike from the peak of aboveground nuclear testing at 5 cm in the 1991 core anchors the ^{210}Pb chronology at 1963. We applied the 1991 core chronology to the 2004 mud–water interface core by matching diatom time series in both cores (Steinitz-Kannan et al., 1998). The diatom data indicate 1 cm of sediment was deposited between 1991 and 2004.

For the radiocarbon chronology, we pretreated 17 bulk sediment samples, subsampled at 20 cm intervals, with the standard acid–base–acid procedure of diluted HCl and NaOH to remove any carbonates and soluble organic material (Hedges et al., 1989). Samples were combusted at the University of Arizona Accelerator Mass Spectrometry (AMS) facility. One additional bulk sediment sample was combusted at INSTAAR Laboratory for AMS Radiocarbon Preparation and Research by Dr. Z. Zhang. We calculated calibrated ages and 2σ errors for each sample with Calib 5.0 using the Southern Hemisphere dataset (Stuiver and Reimer, 1993; McCormac et al., 2004). The two post-bomb radiocarbon ages at the top of the core were calculated using the online program CALIBOMB (Reimer et al., 2004). Our calibrated ages are the mean value of selected 2σ calibration age ranges. We chose the most probable 2σ age range (in the case where there was more than one) for each age based on consistency with the ages and sedimentation rates calculated from the ^{210}Pb data and those ^{14}C ages with only 1 calibration age range. We plotted the ^{210}Pb, ^{137}Cs, and calibrated radiocarbon ages and corresponding depths together and fit the data with a smooth curve function to interpolate individual sample ages on a 1 cm scale (Fig. 3). We interpolated 2σ age model error for each sample depth; 2σ age model errors are rounded to the nearest decade. To assess the degree of the reservoir effect in El Junco, we also obtained fraction modern carbon ($F^{14}C$) values for two submerged plants and one unsubmerged plant from the El Junco shoreline.

3.3. Grain size and C/N procedures

We pretreated sediment samples for grain size analysis at 1 cm intervals using a modification of the methods given by Dr. Donald Rodbell of Union College (http://www1.union.edu/rodbelld/grainsizeprep.htm) with 10% HCl to remove carbonate, 30% H_2O_2 to remove organic matter, and 1 M NaOH to remove biogenic silica (diatoms and phytoliths), centrifuging and decanting sediment samples three times between each step. We then added $(NaPO_3)_6$ to the samples to ensure clay-sized particles would not aggregate. Using a laser-diffraction particle size

Table 2
El Junco age model data, including radiocarbon, ^{210}Pb, and ^{137}Cs measurements and associated ages

Lab no.	Type	Depth (cm)	δ^{13}C (‰)	FMC	^{14}C age, 1s error	Selected 2s cal. age range	Cal. age used in study*	^{210}Pb 2s error (year)	Notes
AA61609	^{14}C		−33.1	1.0767±0.0044	Post-bomb				Aquatic plant—*Hydrocotyle*
AA61610	^{14}C		−32.56	1.0684±0.0044	Post-bomb				Aquatic plant—*Juncus*
AA61611	^{14}C		−33.26	1.0784±0.0044	Post-bomb				Terrestrial plant—*Darwiniothamnus*
AA63507	^{14}C	0.5	−27.99	1.1332±0.0083	Post-bomb	1991.54–1996.98 AD	10		Age calculated using CalibBomb
AA63508	^{14}C	1	−28.36	1.1430±0.0083	Post-bomb	1990.57–1994.74 AD	11		Age calculated using CalibBomb
Univ. Florida	^{210}Pb	2					18	1.1	
Univ. Florida	^{210}Pb	4					26	1.2	
Univ. Florida	^{210}Pb	6					37	1.3	
Univ. Florida	^{137}Cs	6					41		
Univ. Florida	^{210}Pb	8					52	1.8	
Univ. Florida	^{210}Pb	10					68	2.3	
Univ. Florida	^{210}Pb	12					79	3	
Univ. Florida	^{210}Pb	14					93	4.1	
Univ. Florida	^{210}Pb	16					102	4.8	
Univ. Florida	^{210}Pb	18					114	5.9	
AA62397	^{14}C	44	−28.8	0.9450±0.0044	455±38	329–377	350		
MIT	^{14}C	51	−27.2	0.9514±0.0026	400±25	433–495	460		
AA62398	^{14}C	64	−27.93	0.9157±0.0049	707±43	557–672	610		
AA62399	^{14}C	84	−26.3	0.8643±0.0043	1171±40	935–944	940		
AA62400	^{14}C	104	−26.52	0.8575±0.0044	1235±42	974–1182	1080		
AA62401	^{14}C	122	−27.69	0.8379±0.0041	1420±40	1230–1350	1290		
AA62402	^{14}C	144	−25.4	0.7908±0.0039	1885±40	1691–1873	1780		
AA62403	^{14}C	164	−21.57	0.7526±0.0039	2283±42	2140–2342	2240		
AA62404	^{14}C	184	−26.76	0.7120±0.0034	2729±38	2740–2859	2800		
AA62405	^{14}C	204	−20.45	0.7040±0.0037	2820±42	2763–2961	2860		
AA62406	^{14}C	208	−22.72	0.6927±0.0048	2949±55	2868–3212	3040		
AA62407	^{14}C	228	−30.82	0.6347±0.0039	3652±50	3722–3799	3760		
AA62408	^{14}C	248	−29.15	0.6166±0.0035	3855±46	4138–4412	4280		
AA62409	^{14}C	268	−29.38	0.5585±0.0032	4679±47	5273–5477	5380		
AA62410	^{14}C	288	−30.05	0.4935±0.0034	5674±55	6291–6507	6400		
AA62411	^{14}C	308	−29.51	0.4457±0.0025	6491±45	7269–7429	7350		
AA62412	^{14}C	328	−22.65	0.3900±0.0023	7564±47	8273–8402	8340		
AA62413	^{14}C	348	−31.87	0.3620±0.0022	8162±49	8970–9259	9110		

analyzer (Malvern Mastersizer, 2000) coupled to a Hydro 2000S sample dispersion accessory, we took five consecutive measurements on each sample and averaged the results, stirring the samples at 3500 rpm with 70% sonication for 1 min prior to measurement and during measurement. We report results as volume percent clay (<3.9 μm diameter), silt (3.9–62.5 μm diameter), and sand-sized (62.5–2000 μm diameter) particles for each sample. We subsampled sediment for C/N analysis every 3.5 cm within the top 120 cm of the core, and every 7.0 cm for the remainder (233 cm) of the core. We pretreated the samples with 6% sulfurous acid in silver capsules to remove any carbonate and dried them in a 40 °C oven after Verardo et al. (1990). We measured the carbon and nitrogen contents of the bulk sedimentary organic matter in the Stable Isotope Laboratory at the University of Arizona using a Costech elemental analyzer coupled to a continuous flow gas-ratio mass spectrometer (Finnigan Delta PlusXL). Standardization of elemental analysis is based on acetanilide with a precision of 0.15%.

3.4. Lake model

We simulated monthly changes in El Junco lake level with a simple, transient model after Shanahan et al. (2007) to evaluate how El Junco might respond to ENSO-forced changes in surface climatic variables. Change in lake level is a function of changes in precipitation, evaporation, runoff and discharge from the lake catchment area, given by the equation:

$$\Delta H = \frac{P + R - E - D}{\Delta A} \quad (1)$$

where ΔH is the change in lake level, P is precipitation, R is runoff, E is evaporation, D is discharge, and ΔA is change in lake surface area (Shanahan et al., 2007). We calculated a surface area–maximum depth relationship for the lake using a previously published map of El Junco (Colinvaux and Schofield, 1976a):

$$\text{Surface area } (m^2) = -1 \times 10^{-11}(\text{lake depth})^3 + 1710.4(\text{lake depth})^2 + 2 \times 10^{-10}(\text{lake depth}) \quad (2)$$

Because there are no meteorological records at El Junco, we estimated monthly total precipitation in the model using an average of total precipitation (in mm month^{-1}) on the coasts of Santa Cruz Island from 1965 to 1998 and San Cristobal Island from 1951 to present (Baker et al., 1994; Snell and Rea, 1999). It was necessary to average these two datasets together due to temporal gaps in the San Cristobal data, but they are well correlated ($r = 0.90$). Data on long-term evaporation rates near the site are limited, and only sparse pan evaporation data (mm month^{-1}) exist from the coast of San Cristobal between 1987 and 1996. Therefore, evaporation needs to be independently estimated. To parameterize evaporation, the model uses a modified version of the Penman (1948) potential evaporation equation for open water (Shuttleworth, 1993; Shanahan et al., 2007):

$$E_p = \frac{\Delta}{\Delta + \gamma} A + \frac{\gamma}{\Delta \times 6.43(1 + 0.336U)/\lambda} D \text{ mm day}^{-1} \quad (3)$$

where E_p is potential evaporation (mm day^{-1}), A is the energy available for evaporation (MJ m^{-3} day^{-1}), D is the vapor pressure

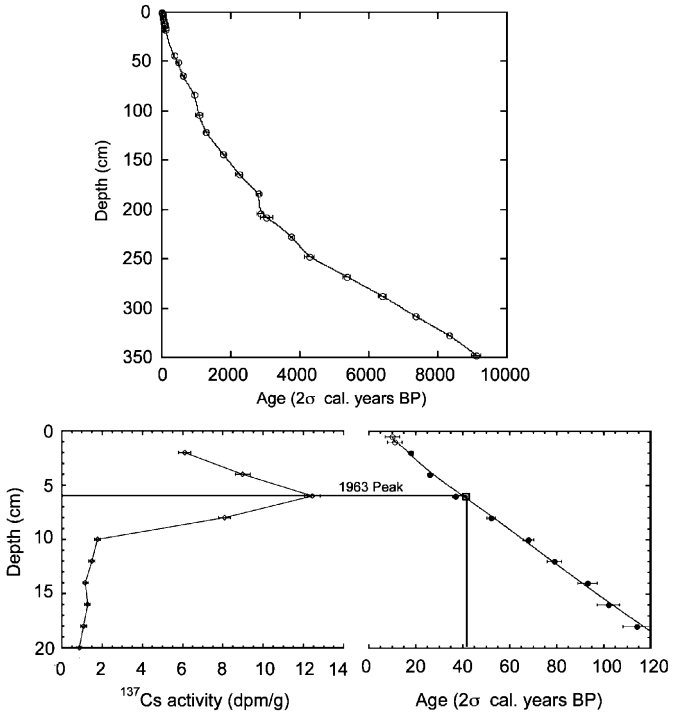

Fig. 3. (A) El Junco age model, including radiocarbon, ^{210}Pb, ^{137}Cs, and post-bomb ^{14}C ages. (B) ^{137}Cs bomb-spike and its associated placement in the age model curve, and inset of ^{210}Pb and two ^{14}C post-bomb dates in upper 20 cm of El Junco sediment record. Open circles are post-bomb radiocarbon, open square is the ^{137}Cs bomb-spike, and filled circles are ^{210}Pb ages.

deficit (kPa), U is the mean wind speed ($m\,s^{-1}$), γ is the psychrometric constant ($kPa\,^{\circ}C^{-1}$), and λ is the latent heat of water vaporization ($MJ\,kg^{-1}$). The slope of the saturated vapor pressure versus temperature curve is expressed by Δ (Shuttleworth, 1993; Shanahan et al., 2007). For a more complete discussion of the model, see Shanahan et al. (2007). A is computed using an energy budget model, and depends on the net energy transferred to the lake by solar irradiance, and is strongly modified by seasonal changes in hours of sunshine (which can be computed directly), as well as by changes associated with cloudiness. Fractional cloudiness data were obtained from the International Satellite Cloud Climatology Program (ISCCP) for 1.25°S, 89.75°W for the years 1983–1997 (Rossow et al., 1996). We predicted monthly fraction cloudiness values prior to this interval using a regression between measured fraction cloudiness and air temperature at El Junco between 1983 and 1997:

$$\text{Fraction cloudiness} = 0.03 \times (\text{El Junco temperature}) - 0.20, \quad r = 0.51 \tag{4}$$

Similarly, vapor pressure deficit measurements (from the NOAA National Centers for Environmental Prediction/Climate Prediction Center Global Summary of the Day) are temporally sparse, so we estimated monthly D values using a regression between measured D and temperature at El Junco:

$$D\,(\text{mb}) = 0.54 \times (\text{El Junco temperature}) - 2.66, \quad r = 0.58 \tag{5}$$

Wind speeds were taken from monthly 1950 to 1997 COADS surface wind speed in $m\,s^{-1}$ for 1°S, 89°W, the grid cell containing San Cristobal.

A key component of many of the evaporation model parameters is water temperature (T_w). There are no consecutive monthly measurements of El Junco water temperature, so we replaced T_w with monthly air temperature, T_a, assuming that although water temperature will lag air temperature due to the higher specific heat of water, the two are closely related. Since air temperature has not been measured at El Junco prior to 2005, we estimated El Junco temperature using average coastal temperature for the Galápagos and an empirical lapse rate of 9 °C per 1000 m derived from contemporaneous half-hourly measurements at Bainbridge Rocks (sea level) and El Junco (675 m a.s.l.) throughout 2005 (W. Gosling, personal communication).

There is clearly uncertainty in our evaporation estimates, but we are limited by the available data. However, our calculated evaporation estimates are similar in magnitude to the limited pan evaporation data for the Galápagos (Fig. 4). The evaporation values should be regarded as maximum estimates for El Junco, given that evaporation in the highlands of San Cristobal is likely lower than evaporation at the coast due to the stratocumulus cloud cover at higher elevations.

The model computes runoff as the amount of precipitation falling into the catchment area minus evapotranspiration from the catchment (Shanahan et al., 2007). Evapotranspiration is not measured, so we estimate it here using the reference crop evaporation rate (Shuttleworth, 1993), which should be a good approximation for the low shrubs and grasses present at the site. The reference crop evaporation rate uses A, the energy available for evaporation, D, the vapor pressure deficit, temperature, wind speed, and the elevation of the site (for more details, see Shanahan et al., 2007).

We ignored groundwater discharge from the basin floor in this simple model, as there is no information on the residence time of the lake water. The lake is closed, but there could be some discharge from the bottom of the basin, although it is probably constant and independent of climate. To account for discharge through the overflow channel on the crater rim, the simulated lake was only allowed to reach the outflow level of 6 m. All water above this level is assumed to flow out of the overflow outlet.

To estimate the sensitivity of El Junco lake level to El Niño frequency and intensity, we modeled changes in lake level for weak/moderate and strong/very strong El Niño events at periods ranging from 2 to 24 years over a 50-year time interval. Simulated El Niño events lasted 1 year, although El Niño events in the instrumental record can be shorter or longer. Using available data from 1951 to 1997, we represented weak/moderate El Niño months as an average of those months of climate data (precipitation, temperature, etc.) when Niño 1+2 SST anomalies value range from 0.5 to 1 °C. Strong/very strong El Niño months were represented by the average of those months with a Niño 1+2

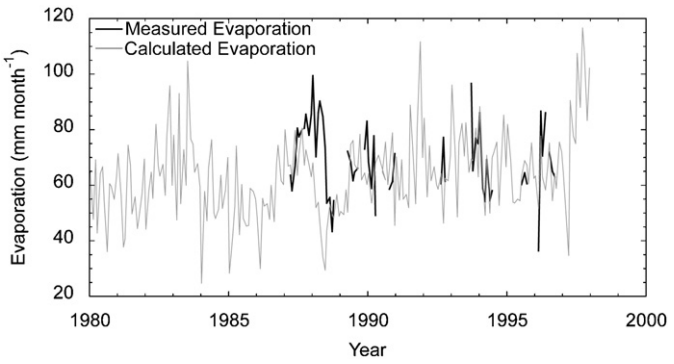

Fig. 4. Pan evaporation measurements (thick black line) from San Cristobal, in $mm\,month^{-1}$ for 1980–1997, and evaporation estimates (thin gray line) for El Junco, calculated using the Penman (1948) evaporation equation for open water.

SST anomaly value greater than 1 °C. We used the Niño 1+2 SST index as it is closest to the Galápagos and because the origin and propagation direction of El Niño events varies across the central and eastern equatorial Pacific, bringing warmer SST (and rainfall) to the central and eastern tropical Pacific in different months. To investigate the effect of different background conditions on the lake's response to El Niño events, the climate data representing the months between El Niño events are represented in two separate simulations as either La Niña-like or strongly La Niña-like. Months with a Niño 1+2 SST anomaly less than 0.5 °C are considered La Niña-like, whereas months with a Niño 1+2 SST anomaly less than −0.5 °C are considered to represent strong La Niña conditions. Results are expressed as changes in the mean lake level and minimum lake level given different periodicities of El Niño events. Mean lake level is calculated as the average lake level of the 50 years (600 months) in a given simulation. Minimum lake level is the lowest lake level during the 50 years (600 months) of a given simulation.

4. Results

4.1. Lake sediment results

The bottom of our El Junco core (3.5 m) dates to 9200±160 cal years BP. We observe relatively stable sedimentation rates and no radiocarbon age inversions (Fig. 3). The $F^{14}C$ of the terrestrial (1.0784±0.0044) and aquatic (1.07255±0.0044) plant samples are within error of each other, so we conclude there is no lake carbon reservoir effect in El Junco. The mean sedimentation rate for the entire El Junco record is 0.04 cm $year^{-1}$, giving an average resolution of 25 years for our 1 cm sampling intervals.

The stratigraphy of the El Junco core can be divided into several sections based on macroscopic features observed on the split cores (Schnurrenberger et al., 2003). From the top of the core to 1.3 m (to −1500±70 cal years BP), the sediment is brown-red, massive, organic-rich silt. From 1.3 to 2.1 m (1500±70 to 3100±170 cal years BP), the sediment is brown-red, laminated, organic-rich silt. From 2.1 to 2.4 m (3100±170 to 4100±110 cal years BP) the core is composed of red, laminated clay with strongly contrasting black-brown and brown-red cm-scale laminations. The sediment interval from 2.4 to 3.1 m (4100±110 to 7500±110 cal years BP) is also composed of red, laminated clay but with a combination of thick and thin, more irregularly spaced, brown-red laminations. A 10 cm interval of finer (mm-scale) black-brown and brown-red laminations occurs from 2.85 to 2.95 m (6200±110 to 6700±100 cal years BP). There is a return to thicker, brown-red banding from 2.95 to 3.1 m (6700±100 to 7500±80 cal years BP), and red-brown, massive, clay from 3.1 to 3.2 m (7500±80 to 7900±70 cal years BP). From 3.2 to 3.4 m (7900±70 to 8800±90 cal years BP), the core is composed of red-brown, faintly laminated clay. From 3.4 to 3.5 m (8800±90 to 9200±160 cal years BP) the core consists of red-brown and black, laminated clay, ending in a 3 cm black, massive, organic-rich unit.

Our El Junco paleoenvironmental record consists of two independent types of proxy data. First, C/N variations provide a measure of the amount of terrestrial versus aquatic organics in the lake sediment. Terrestrial plant C/N ratios are higher than aquatic plankton C/N ratios, due to greater amounts of nitrogen in phytoplankton and the presence of cellulose in terrestrial organic matter (Meyers and Ishiwatari, 1993). Land plants usually have C/N values greater than 20, with values ranging from 20 to greater than 500, whereas plankton have C/N values less than 10 (Meyers and Ishiwatari, 1993; Meyers, 1994). Thus, lower C/N values preserved in lake sediments indicate a significant plankton contribution to the preserved organic matter, whereas higher C/N values suggest a greater amount of land-derived organic matter. There is a strong trend in C/N values over the Holocene, with decreasing values toward present (Fig. 5). Millennial variations are also prominent in the C/N time series: C/N values are higher and more variable from 9200±160 to 6000±110 cal years BP (mean = 30, S.D. = 8), with an abrupt, step-like shift to lower values at 5600±100 cal years BP. Values then remain low and less variable from 5600±100 to 4200±130 cal years BP (mean = 17, S.D. = 2). A period of higher C/N values occurs from 4200±130 to 3200±160 cal years BP (mean = 24, S.D. = 3). After 3200±160 cal years BP, C/N values remain low until present (mean = 17, S.D. = 6), although there is one apparent outlier (= 52) at 2360±100 cal years BP. Removing this outlier reduces the mean C/N value to 16 and the standard deviation to 3 for 3200±160 cal years BP to present. The individual % organic carbon (C) and % nitrogen (N) time series that comprise the C/N record indicate an upward trend in % N from 4000 cal years BP to present (Fig. 5). C abundance is more variable than N abundance throughout the record, ranging from 8% to 66%, whereas % N ranges from 0.3% to 3%. The C/N outlier at 2360±100 cal years BP is due to high C abundance (66%).

We also use grain size data in the El Junco core as a proxy for tropical Pacific climate variability during the Holocene. Grain size variability in a lake sediment core can indicate changing transport energy, lake levels, and paleoenvironmental zones of deposition. Three classes of sediment particle size (percent clay, silt and sand) exhibit considerable variability over the length of the El Junco record. The abundance of clay and silt is more variable from 9200±160 to 5600±100 cal years BP (S.D. = 12%). After 5600±100 cal years BP percent clay gradually increases while percent silt decreases, culminating in high percent clay values (mean = 54%, S.D. = 7%) and low percent silt values (mean = 43%, S.D. = 6%) between 3800±40 and 3200±160 cal years BP. There is then a two-step transition to lower percent clay and higher percent silt at 3200±160 and 2000±100 cal years BP (Fig. 5). From 9200±160 to 9000±120 cal years BP, percent sand is high (mean = 10%, S.D. = 4%), and then remains low (mean = 2%, S.D. = 2%) from 9000±120 to 4200±130 cal years BP. At 4200±130 cal years BP, sand variability increases, with abrupt transitions to larger values. There is a dramatic increase in sand abundance at 2000±100 cal years BP, and values remain relatively high until 1500±70 cal years BP (mean = 17%, S.D. = 6%).

The trends in the C/N, silt, and clay time series all show trends from the mid-Holocene to present, with increasing silt abundance, decreasing clay abundance, and decreasing C/N values (Fig. 5). The abrupt, step-like decrease in C/N values at 5600±100 cal years BP is also evident in the clay and silt time series. The two-step transition at 3200±160 and 2000±100 cal years BP is also present in both the silt and clay time series, and the shift at 2000±100 cal years BP marks the onset of increased sand abundance that lasts until 1500±70 cal years BP. The initial onset of higher, more variable sand abundance at 4200±130 cal years BP also coincides with a period of high C/N and clay values and low silt values.

4.2. Model results: simulating the response of El Junco to ENSO conditions

Simulated mean and minimum El Junco lake level varies strongly in response to different El Niño event strengths and periodicity (Fig. 6). With more frequent El Niño events of either strength, mean lake level is higher and the lake is permanent. The

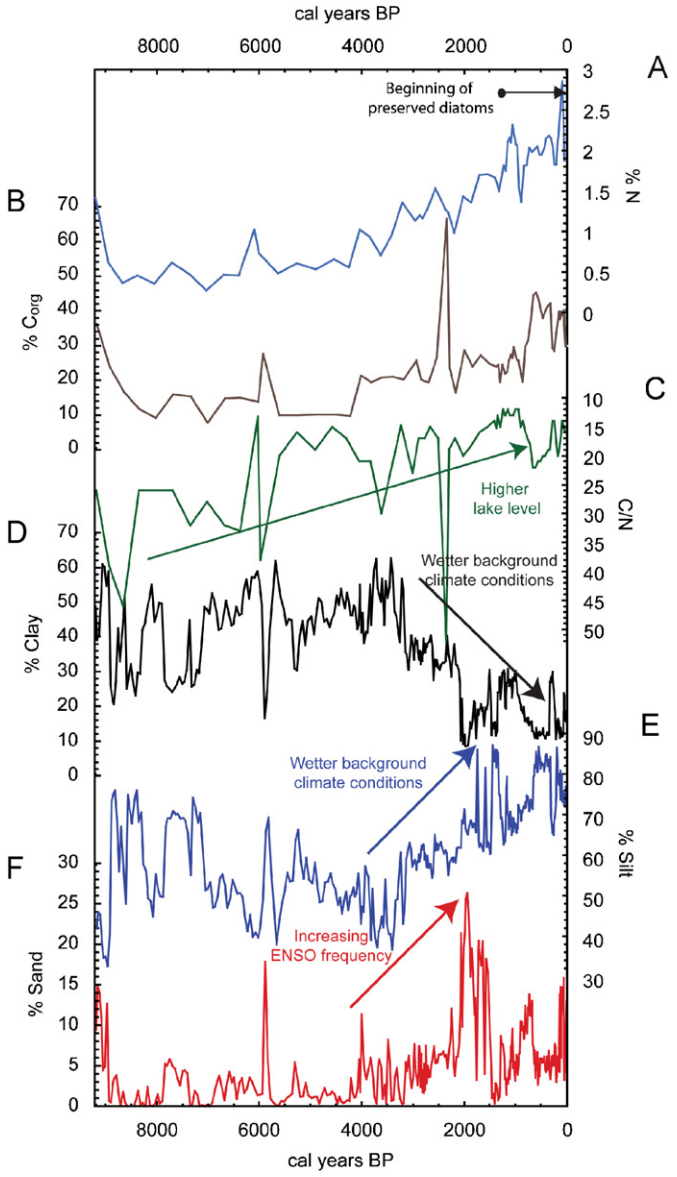

Fig. 5. El Junco carbon, nitrogen, and grain size (volume percent clay, silt, and sand) values, 9200 cal years BP to present. (A) Percent nitrogen. (B) Percent organic carbon. (C) C/N values. (D) Percent clay. (E) Percent silt. (F) Percent sand. Arrow at top indicates period of preserved diatoms in El Junco core beginning at 1250±70 cal years BP.

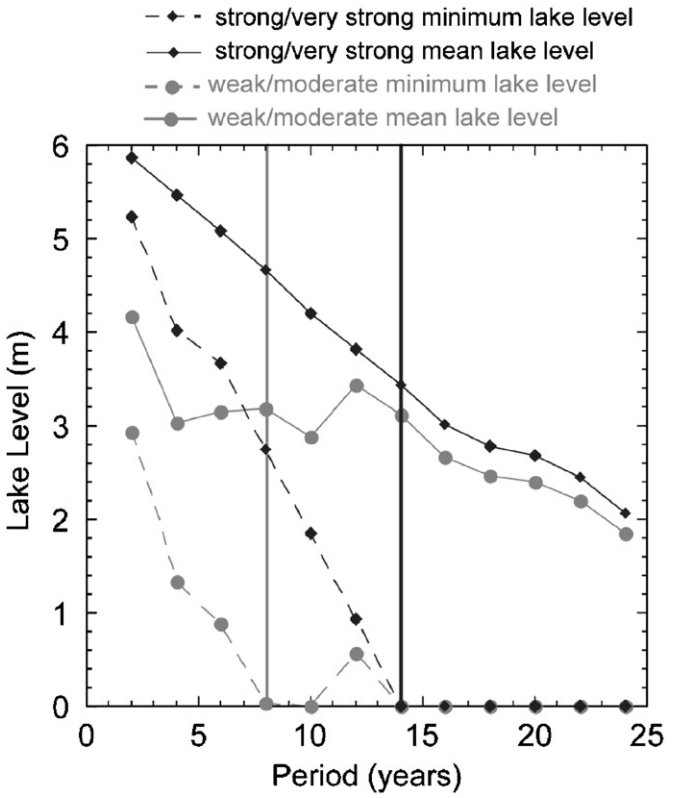

Fig. 6. Simulated El Junco lake level for varying El Niño event magnitude and period, with mean (solid line) and minimum (dashed line) lake levels for weak/moderate (gray) and strong/very strong (black) El Niño events. Vertical lines denote the El Niño periodicity at which El Junco likely dries out for simulations using weak/moderate (gray) and strong/very strong (black) events. Data are only plotted for the simulation with intervening, non-El Niño months represented by "La Niña" Niño 1+2 values ($<0.5\,^{\circ}C$). The simulation with intervening, non-El Niño months represented by cooler, "strong La Niña" Niño 1+2 values ($<-0.5\,^{\circ}C$) gave similar results.

increase in lake level is due primarily to increased precipitation and runoff. Evaporation is also higher during El Niño events, as the low-lying stratocumulus clouds characteristic of cold SSTs dissipate and there is more sunlight, but increased precipitation is more important than increased evaporation in controlling lake level. As El Niño event frequency decreases, mean lake level also declines and the lake becomes ephemeral. Our results also suggest that there is little difference in mean or minimum lake level when the months in between El Niño events are represented by stronger or weaker La Niña conditions, indicating it is the amount of rain from El Niño events and the frequency of those events that controls lake level, at least in the period of instrumental data. When the years between El Niño events are colder, mean lake level is an average of 0.1 m lower for strong/very strong events and 0.03 m lower for weak/moderate events. This slight difference is likely due to the lower amount of seasonal rainfall associated with colder SST. The simulated relationship between lake level and El Niño periodicity estimates the El Niño period at which El Junco likely dries up, shown by the vertical lines in Fig. 6. For strong/very strong events, we estimate that El Junco dries out at an El Niño period of 14 years, and for weak/moderate events, El Junco initially dries out at an El Niño period of 8 years. For weak/moderate events, mean and minimum lake level increase slightly at the 12-year period. It is unclear what is driving this small increase in lake level, since less frequent El Niño precipitation leads to lower lake levels at other periodicities. However, both the 10-year and 12-year period simulations have the same number of El Niño events in the 50 years of the model run (at years 0, 10, 20, 30, and 40, and at years 0, 12, 24, 36, and 48, respectively). The increase in mean and minimum lake levels the 12-year periodicity may be due to the spacing of the events. Regardless, we conclude that to maintain permanent water in El Junco, there likely must be an El Niño event every 8–14 years, depending on the event strength.

Although we did not model the response of El Junco lake level to longer-term (e.g., multidecadal to millennial) variations in eastern tropical Pacific climate, it is possible that secular changes in background climate larger than those modeled by the La Niña conditions drive changes in El Junco lake level. Independent of El Niño event frequency, a long-term weakening of the Walker Circulation would lead to increased SST, convection, and precipitation in the eastern tropical Pacific, likely leading to increased El Junco lake levels. Similarly, a long-term strengthening of the Walker Circulation would lead to decreased SST, convection, and precipitation in the eastern tropical Pacific, and hence lower El

Junco lake levels. Long-term shifts in the position of the Intertropical Convergence Zone (ITCZ) could also affect El Junco lake levels via changes in the strength and persistence of the southeasterly trade winds (Mitchell and Wallace, 1992; Koutavas et al., 2006). A more southerly displaced ITCZ could weaken these trade winds, also leading to increased SST, convection, precipitation, and higher El Junco lake levels. Conversely, a more northerly ITCZ could strengthen the trade winds, leading to lower SST, convection, precipitation values and therefore lower El Junco lake levels.

5. Discussion

5.1. The El Junco record and tropical Pacific climate variability

The El Junco records of C/N and grain size variability are indicators of significant changes in lake level and eastern tropical Pacific climate over the Holocene. Initial paleolimnological investigations at El Junco cited grain size as evidence for variations in lake level. Colinvaux (1972) originally interpreted clay-dominated sediments in El Junco as evidence of a dry basin. This interpretation was supported by the absence of clay minerals that form in the presence of water (e.g., montmorillonite, illite, and goethite) and evidence for oxidation during periods of high clay deposition (Colinvaux, 1972). We also interpret the greater amount of clay-sized particles in the early to mid-Holocene portion of the El Junco sediment record as evidence of a frequently dry lakebed, with particularly dry episodes occurring prior to 6000 ± 110 cal years BP, at 5600 ± 100 cal years BP and between 3800 ± 40 and 3200 ± 160 cal years BP. The abrupt, two-step transition to larger, silt-sized particles at 3200 ± 160 and 2000 ± 100 cal years BP is thus evidence of a two-step transition to a state characterized by higher lake levels. Other investigations into the controls on lacustrine grain size variability suggest that increased precipitation in closed-basin lake catchments transports larger grains from the catchment into the center of the basin, with grain size in the sediment a function of the intensity and/or amount of rainfall (Sun et al., 2002; Chen et al., 2004). Our lake modeling indicates that increased precipitation leads to higher lake level in El Junco, so the observed increase in silt-sized particles relative to clay-sized particles from the mid-Holocene to present suggests increasing precipitation and lake levels.

Silt abundance generally mirrors changes in clay abundance ($r=-0.94$), but percent sand variability has a distinctive pattern of temporal variability ($r=-0.54$ with clay, 0.23 with silt), suggesting that it is decoupled from the other proxies. We hypothesize that changes in sand content may reflect changes in the intensity of rainfall. In contrast, clay and silt variability likely reflects changes in the overall amount of precipitation from changes in both El Niño events as well as seasonal rainfall. In previous lake sediment studies from the eastern tropical Pacific, large precipitation events associated with El Niño are hypothesized to enhance deposition of siliciclastic sediments from the catchment area, identified as distinctive layers in the sediment cores (Moy et al., 2002; Riedinger et al., 2002). In the El Junco core, we do not have the temporal resolution to identify layers representative of individual El Niño events, but given our hypothesis that grain size is related to the intensity and amount of rainfall, we interpret increases in sand abundance as an increase in the number of intense rainfall events associated with El Niño events. Rainfall associated with El Niño in the Galápagos can be an order of magnitude larger than average seasonal rainfall (Fig. 2). Thus, the increases in sand variability in the interval between 9200 ± 160 and 9000 ± 120 cal years BP and after 4200 ± 130 cal years BP likely indicate increases in ENSO frequency and/or magnitude. From 9200 ± 160 to 9000 ± 120 cal years BP and 3800 ± 40 to 3200 ± 160 cal years BP, increased sand content in conjunction with more clay relative to silt suggest that there were more El Niño events coupled with cooler, drier background conditions in the eastern tropical Pacific. In contrast, between 2000 ± 100 and 1500 ± 70 cal years BP, when we observe the highest sand abundance and infer the period of highest ENSO variance in our record along with greater amounts of silt elative to clay, we hypothesize that there were more El Niño events with warmer background conditions. It is important to note our estimates of changes in ENSO frequency are qualitative, since we do not have a quantitative relationship between modern instrumental climate data and grain size due to the low resolution of the sediment record compared to the instrumental record.

It is possible to constrain the relationships between grain size and instrumental climate of the last 100 years if regional climate data are temporally averaged to the resolution of the grain size data (Fig. 7). From 1944 to 1976, clay abundance is high when SST and Niño 1+2 values are lower, and from 1976 to 2004, clay abundance is low when SST and Niño 1+2 values are higher. Although clay and silt are inversely correlated through the Holocene, they are not significantly correlated during the last 100 years ($r=-0.19$). From 1944 to 1970, silt abundance is low and SST is cool, whereas from 1976 to 1982 silt abundance is high while SST is warm. However, silt abundance declines from 1982 to 2004 while SST and Niño 1+2 values increase. This may be due to the two extreme El Niño events during this time period (1982/1983 and 1997/1998), the intensity of which may have led to increased sand deposition; percent sand increases from 1982 to 2004 along with SST and Niño 1+2 values. Sand abundance is also low from 1957 to 1982 during a period of lower SST and higher from 1938 to 1951 during a period of warmer SST. Prior to 1940, the relationship between grain size and SST weakens. This is likely due to the existence of a large ranching/farming plantation (Hacienda El Progreso) operated in the highlands of San Cristobal beginning in 1879, and we interpret the weakened grain size–climate relationship to be a result of grazing and erosion around El Junco in the earlier part of the 20th century (LaTorre, 1999). Colinvaux and Schofield (1976a) also noted that highlands around El Junco were rangeland for ~5000 cattle into the 1960s, although the area around the crater was fenced off during our visit in 2004.

C/N values confirm our interpretation of the grain size data through the Holocene. Higher C/N values and greater C/N variance in the early to mid-Holocene portion of the El Junco sediment record likely indicate a shallower, more ephemeral lake, with a greater influx of terrestrial organic matter onto the basin floor, whereas lower C/N values later in the Holocene points to increasing algal input due to a more consistently deep lake. The possibility that this linear C/N trend is an artifact of nitrogen loss over time (Cohen, 2003) is not supported by the grain size data, which shows that decreased clay abundance and increased silt abundance accompanies lower C/N values. One of the longest, most consistent periods of low C/N values also occurs during the period of highest % N in the record from 1250 ± 70 cal years BP to present, when we observe preserved diatoms in the sediment core. A period of high C/N values from 4200 ± 130 to 3200 ± 160 cal years BP, indicating lower lake level and increased terrestrial organic input, is also coincident with a period of high clay abundance from 3800 ± 40 to 3200 ± 160 cal years BP, likely indicative of lower lake levels.

Changes in the type or amount of vegetation in the El Junco watershed could influence erosion and deposition of clay, silt and sand, as well as the influx of terrestrial organic matter into the lake. Yet pollen records from El Junco indicate little variation in the types of vegetation surrounding the lake over the last 9000

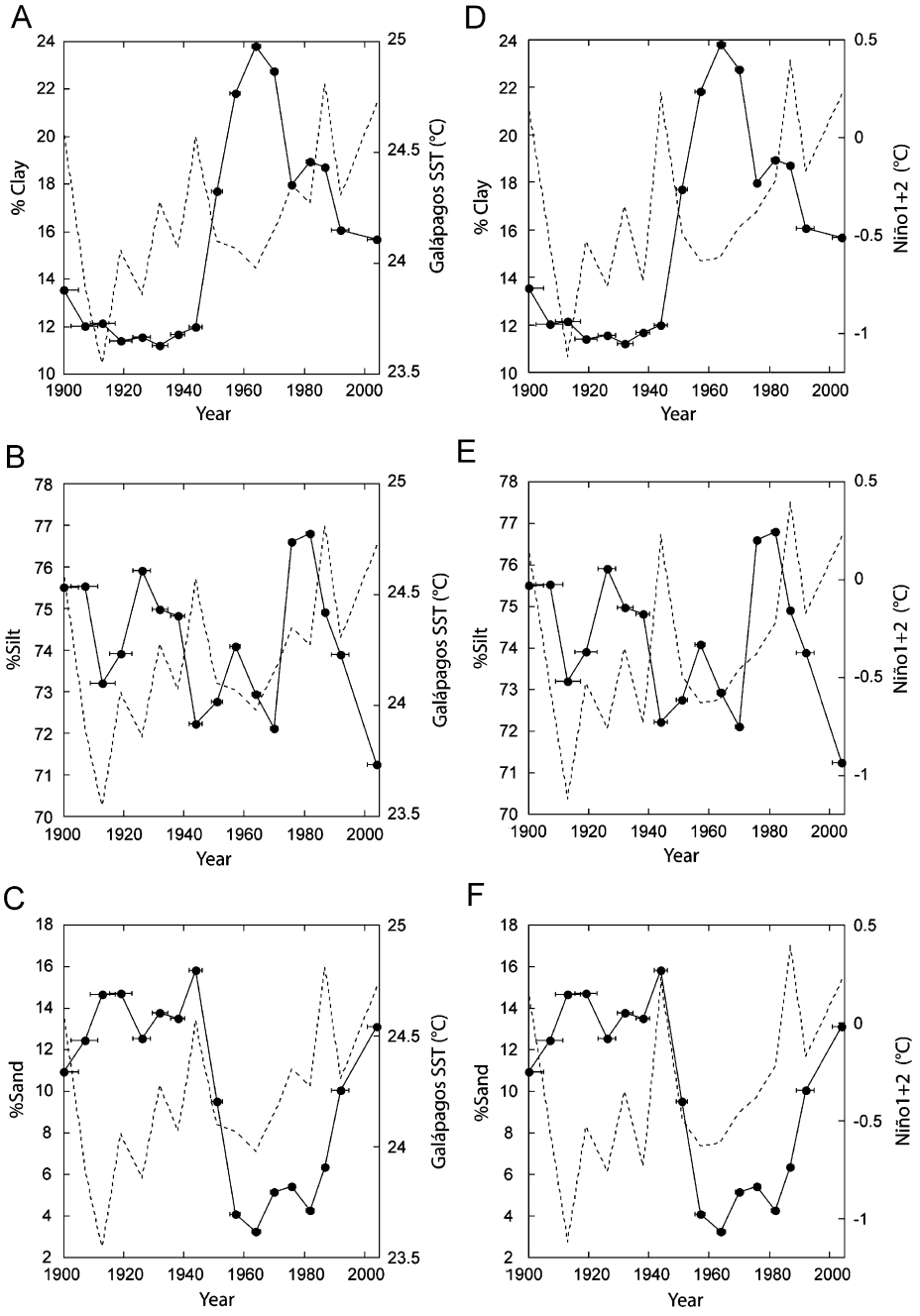

Fig. 7. El Junco grain size (solid lines) and instrumental climate data (dashed lines), 1900–2004 (Smith and Reynolds, 2004). (A) Percent clay and Galápagos SST (°C). (B) Percent silt and Galápagos SST (°C). (C) Percent sand and Galápagos SST (°C). (D) Percent clay and Niño 1+2 SST anomalies (°C). (E) Percent silt and Niño 1+2 SST anomalies (°C). (F) Percent sand and Niño 1+2 SST anomalies (°C).

years. The pollen records also do not give estimates of change in the absolute abundance of plants, but only relative changes in the types of pollen due to low pollen concentration (Colinvaux and Schofield, 1976a, b). However, a record of the spore abundance of the water fern *A. microphylla* indicates El Junco lake level fluctuated throughout the Holocene (Colinvaux, 1972). Colinvaux (1972) interpreted more *A. microphylla* massulae in El Junco sediments as evidence for lower lake levels, since smaller, shallower ponds in the Galápagos are usually covered by *A. microphylla*. The *A. microphylla* record thus suggests a shallow, fluctuating lake prior to 3000 ^{14}C years BP (~2900±500 cal years BP, assuming ±100 years error on the ^{14}C age) and a more permanent, deeper lake from 3000 ^{14}C year BP to present (Colinvaux, 1972). The period of low *A. microphylla* is in general agreement with the grain size and C/N proxies, which also suggest a more permanent, deep lake in the last ~3000 years. In terms of sediment depth, 1.3 m marks the late Holocene decline in *A. microphylla*. This is also near the same depth (1.2 m) that we begin to observe preserved diatoms in the core. Preserved diatoms also suggest a more permanent lake since delicate diatom frustules are easily destroyed when dried and exposed to the atmosphere (Flower, 1993).

5.2. Comparison with records from other tropical sites

Comparing the El Junco grain size record to other Holocene ENSO records, we observe coincident periods of greater ENSO

frequency (Fig. 8). A high-resolution ocean sediment record from near the Peru coast indicates an increase in terrestrial lithic flux, hypothesized to be associated with increased ENSO frequency, before 9000 cal years BP and after ~4500 cal years BP, in agreement with our sand record from El Junco (Rein et al., 2005). Stable isotope values from coastal Peruvian mollusks also indicate El Niño events did occur in the early Holocene from 9000 to 7900 cal years BP (Carre et al., 2005). Pollen evidence from northern Australia also shows increased climate variability after 4000 cal years BP, attributed to an increase in ENSO variability (Shulmeister and Lees, 1995).

Two other ENSO event records, from Bainbridge Crater Lake in the Galápagos and Laguna Pallcacocha, Ecuador, do not suggest ~4200 cal years BP as the time of increased event frequency (Moy et al., 2002; Riedinger et al., 2002). At Bainbridge, where the data only track millennial-scale variations in El Niño event frequency, the authors infer increased ENSO frequency and intensity only after 3100 cal years BP, which is later than the shift in sand at 4200 cal years BP in the El Junco record. At Pallcacocha, the interpreted increase in ENSO frequency occurs much earlier than El Junco or Bainbridge, at 7000 cal years BP (Moy et al., 2002). However, gray-scale record from the same lake does suggest modern ENSO frequency was initiated at 5000 cal years BP (Rodbell et al., 1999). Despite these discrepancies, Bainbridge, Pallcacocha, and the Peru ocean sediment record all suggest the period 2000 to 1000 cal years BP was a period of extremely high, if not the highest, ENSO event frequency during the Holocene, in agreement with the timing of the abrupt increase in sand in the El Junco record and our interpretation of an increase in intense rainfall and ENSO frequency or intensity (Moy et al., 2002; Riedinger et al., 2002; Rein et al., 2005). $\delta^{18}O$ variability in individual foraminifera tests from an ocean sediment core taken near the Galápagos also reveals a larger range of monthly resolution $\delta^{18}O$ values, reflecting enhanced ENSO variability, around 2000 ^{14}C years BP compared to 6000 ^{14}C years BP (Koutavas et al., 2006). Furthermore, windows of annual coral $\delta^{18}O$ variability from Papua New Guinea show damped ENSO magnitude and decreased ENSO frequency from 7600 to 5400 years BP and both extreme (2 times the amplitude of the 1997–1998 event) and prolonged (4–7 years) El Niño events between 2500 and 1700 years BP (Tudhope et al., 2001; McGregor and Gagan, 2004). Another coral $\delta^{18}O$ record from Christmas Island also reveals an extreme El Niño event (2 times the amplitude of the 1997–1998 event) in a 16-year period dated to 1700 years BP (Woodroffe et al., 2003).

Several tropical Pacific SST reconstructions also support our interpretation of the El Junco record. Two independent SST reconstructions from the eastern tropical Pacific indicate warmer SST after 2000 cal years BP, which would have led to enhanced convection and precipitation in this region (Koutavas et al., 2002; Rein et al., 2005). Comparing these two eastern tropical Pacific SST records with an SST reconstruction from the western tropical Pacific suggests that the tropical Pacific SST gradient may have been reduced between 2000 and 1000 cal years BP (Fig. 8A and B) (Stott et al., 2004). A reduced SST gradient would have led to weakened Walker circulation and weaker easterly winds, perhaps favoring the development of more frequent El Niño events during this time period (Koutavas et al., 2006). This framework is consistent with our evidence from El Junco for more frequent El Niño events during this interval. Similarly, the east–west SST gradient derived from the SST records is largest in the mid-Holocene, when inferred ENSO frequency is reduced in El Junco as well as in other ENSO records. Koutavas et al. (2006) note that the zonal SST gradient begins to decrease around 4000–5000 years ago, approximately coincident with the onset of greater ENSO frequency in the El Junco record.

5.3. Potential drivers of tropical Pacific climate during the Holocene

Changes in seasonal solar insolation likely affected tropical Pacific and ENSO variability during the Holocene. Astronomical calculations indicate boreal summers received more insolation in the mid-Holocene (Berger and Loutre, 1991), making boreal and equatorial summers warmer than present. Using the simplified Zebiak–Cane model (Zebiak and Cane, 1987), Clement et al. (2000) demonstrated that with warmer equatorial summers in the mid-Holocene, a stronger SST gradient developed across the tropical Pacific due to greater heating in the west than in the east, leading to stronger easterly winds and a cooler eastern tropical Pacific. These anomalous winds may have maintained a "La Niña-like" state in the mid-Holocene, hindering the development of El Niño events. Simulations using coupled atmosphere–ocean general circulation models (AOGCMs) support these findings, showing a stronger SST gradient across the tropical Pacific, intensified Walker Circulation, and weaker ENSO variability during the early to mid-Holocene (Liu et al., 2000; Kitoh and Murakami, 2002; Otto-Bliesner et al., 2003; Liu et al., 2004). Our new record supports these climate modeling simulations, since it also indicates a cooler, drier eastern tropical Pacific with fewer El Niño events during the early and mid-Holocene.

It is also possible that insolation-induced shifts in the mean position of the ITCZ drove the observed changes in the eastern tropical Pacific through the Holocene (Koutavas et al., 2006). Today, when the ITCZ is further north during boreal summer, the eastern tropical Pacific experiences its cool/dry season, with strong south-easterly trade winds, oceanic upwelling, cool SSTs and reduced precipitation. When the ITCZ moves south of 10°N during boreal winter, the trade winds weaken and upwelling diminishes, leading to warmer SSTs and increased precipitation in the eastern tropical Pacific (Mitchell and Wallace, 1992). Thus, it is possible that long-term changes in the position of the ITCZ associated with changes in seasonal insolation could have affected Galápagos climate. With warmer boreal summers in the mid-Holocene, the ITCZ maintained a more northerly position, resulting in cooler, drier conditions in the eastern tropical Pacific and the drier conditions we observe in the El Junco record. As perihelion moved from the middle to the end of the calendar year from the mid-Holocene to present, the ITCZ began a march south, bringing warmer and wetter conditions to the eastern tropical Pacific. A proxy record of ITCZ position derived from Ti measurements in the Cariaco Basin indicates this southward shift of the ITCZ beginning 5400 years ago (Fig. 9) (Haug et al., 2001). The Holocene trend toward reduced Ti abundance in the Cariaco Basin record, reflecting decreased continental runoff in northern South America and a southward migration of the ITCZ, coincides with the trend toward wetter conditions suggested by the El Junco silt, clay and C/N records. These coincident trends suggest that as the ITCZ moved south, the region around Cariaco became drier while the Galápagos became wetter. Thus, the increase in silt abundance and decreasing C/N values in El Junco from the mid-Holocene to present are likely a reflection of warmer, wetter background conditions in the eastern tropical Pacific, juxtaposed with an increase in El Niño event frequency.

The Cariaco Basin record also shows increased variance in Ti and inferred ITCZ position beginning 4000 cal years BP (Haug et al., 2001), near the time of increase in El Niño events suggested by the El Junco sand record (Fig. 9). The seasonal cycle is the dominant control on the position of the ITCZ, but ITCZ position is also tied to ENSO, with El Niño events resulting in a southward shift of the ITCZ over the tropical Pacific (Deser and Wallace, 1990). These large shifts in the position of the ITCZ suggested by the Cariaco Ti record beginning after 4000 cal years BP could thus be the result of increased ENSO variability (Haug et al., 2001). Yet the Cariaco record does not show much increase in Ti variance

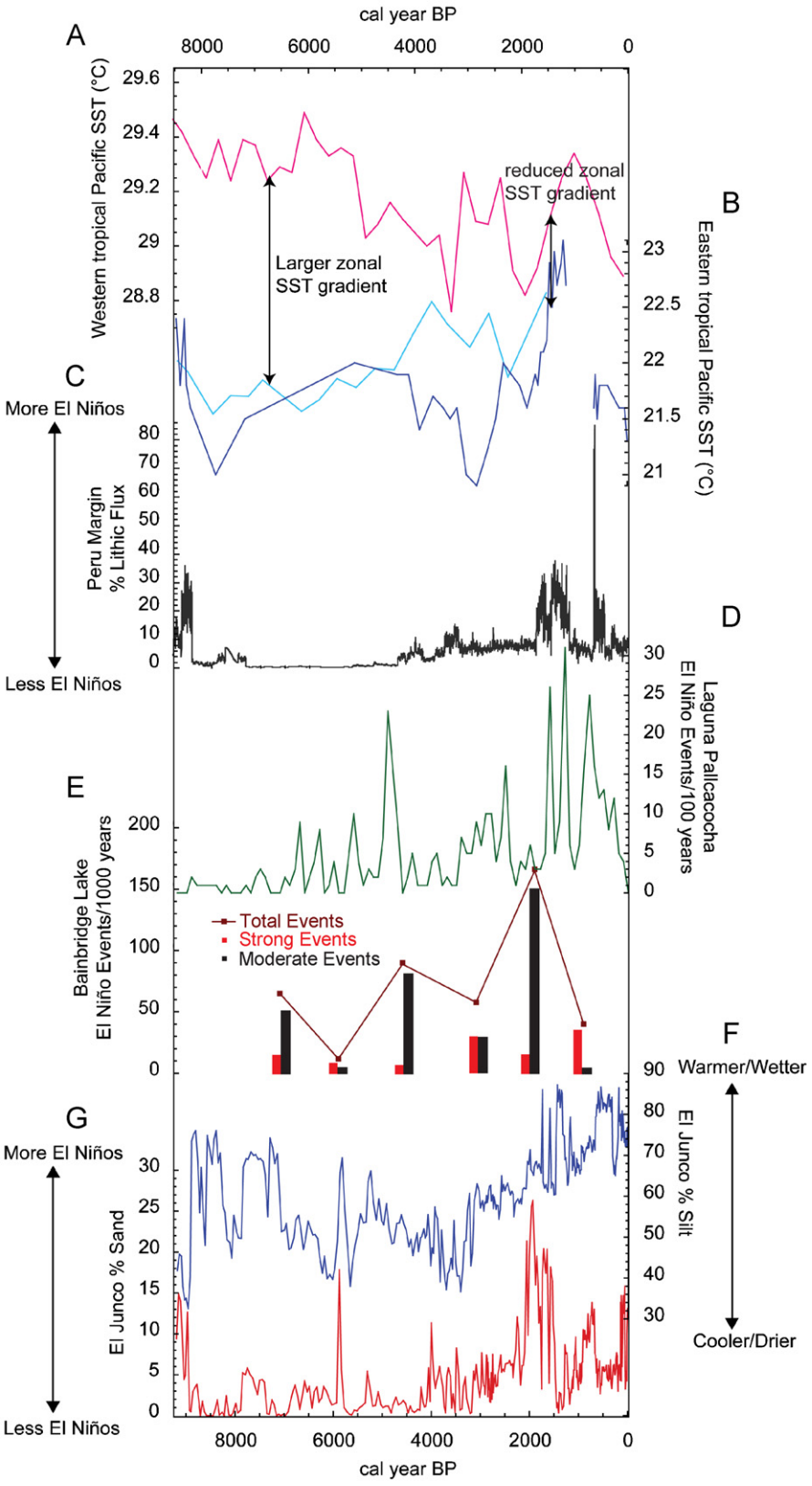

Fig. 8. El Junco grain size records and Holocene ENSO/SST records from the tropical Pacific. (A) Western equatorial Pacific SST (°C) from foraminifera Mg/Ca (Stott et al., 2004). (B) Eastern Equatorial Pacific SST from foraminifera Mg/Ca and alkenones (Koutavas et al., 2002; Rein et al., 2005). (C) Lithic flux (Rein et al., 2005). (D) Laguna Pallcacocha El Niño events/100 years (Moy et al., 2002). (E) Bainbridge Crater Lake El Niño events/1000 years (Riedinger et al., 2002). (F) El Junco silt record. (G) El Junco sand record.

from ~2500 to 1000 cal years BP when seven independent records of ENSO variability indicate a period of much greater ENSO frequency, magnitude, and duration. This suggests a decoupling of ENSO from the North Atlantic ITCZ variability at this time and that other mechanisms must be explored to explain this period of unprecedented ENSO variability.

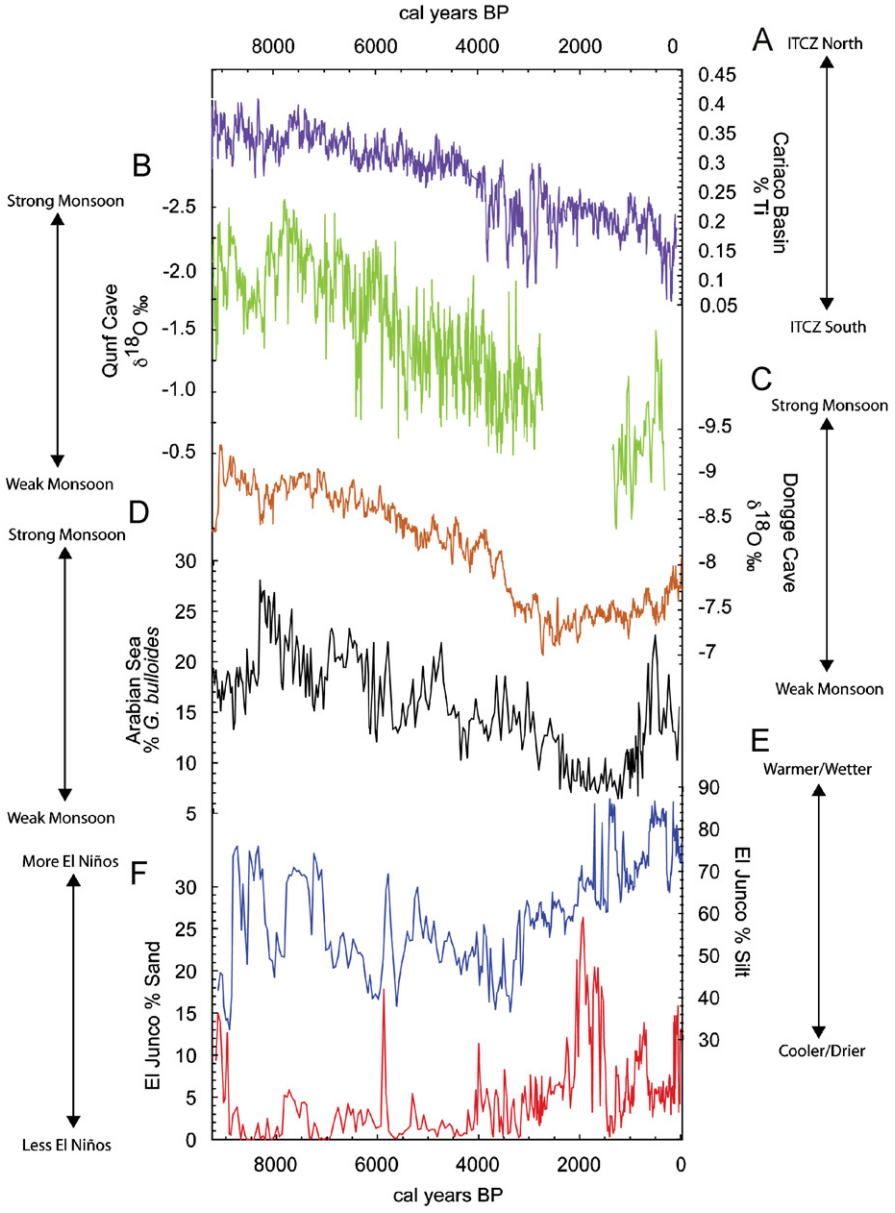

Fig. 9. El Junco grain size records with proxy records of Asian Monsoon variability and ITCZ position. (A) % Ti from the Cariaco Basin, an indicator of ITCZ position (Haug et al., 2001). (B) $\delta^{18}O$ record from Qunf Cave, Oman (Fleitmann et al., 2003). (C) Average of three $\delta^{18}O$ records from Dongge Cave, China (Yuan et al., 2004; Dykoski et al., 2005; Wang et al., 2005). (D) % *Globigerina bulloides* from an ocean sediment core off the coast of Oman, a proxy for Indian Summer Monsoon wind strength (Gupta et al., 2005). (E) El Junco silt record. (F) El Junco sand record.

During the period of instrumental observations, El Niño events tend to coincide with weaker Southwest Asian monsoon rainfall and La Niña events with stronger Southwest Asian monsoon rainfall, although this relationship is not consistent for every ENSO event, and seems to have disappeared in the last few decades (Webster et al., 1998; Kumar et al., 1999). Simulations made with a coupled AOGCM forced by orbitally induced changes in insolation suggest that enhanced Asian monsoon convection in the early and mid-Holocene strengthened Walker Circulation, leading to increased oceanic upwelling and cooler SST in the eastern tropical Pacific, which then further strengthened the Walker Circulation via the coupled ocean–atmosphere Bjerknes mechanisms (Liu et al., 2000). In this modeling study, stronger Asian monsoon-induced Walker Circulation caused weaker El Niño events and less overall ENSO variance at 6000 years BP (Liu et al., 2000). Given that we do not understand the full nature of the monsoon–ENSO relationship at present, it is also possible that the onset of increased ENSO frequency in the mid-Holocene affected monsoon variability, or that the same internal or external forcing drove synchronous changes in both systems (Webster et al., 1998).

There is evidence that variability within the two components of the Asian monsoon, the Southwest (SW) Asian monsoon and East (E) Asian Monsoon, may not be synchronous, complicating a comparison between paleo-ENSO and paleo-monsoon records (An et al., 2000; He et al., 2004). Yet a synthesis of paleo-monsoon records from both the SW and E Asian monsoon regions indicates that in the early to mid-Holocene, when the monsoon was generally stronger, abrupt changes in both regions were synchronous, only becoming decoupled in the last few thousand years (Morrill et al., 2003). A more recent comparison including several new, high-resolution monsoon records from both the SW and E

Asian monsoon regions also indicates millennial-scale homogeneity in the monsoon domains through the Holocene (Fleitmann et al., 2007). Thus, if the Asian monsoon and tropical Pacific are connected on longer time scales, we may expect to see periods of weaker monsoon variability coincident with periods of enhanced ENSO variability beginning around 4200 and between 2000 and 1000 years BP.

Morrill et al. (2003) found that a statistically significant number of both SW and E Asian monsoon records show an abrupt decrease in monsoon strength from 5000 to 4500 cal years BP. However, Fleitmann et al. (2007) find no sign of an abrupt change from 5000 to 4500 years BP in a new compilation of paleo-monsoon records including the Qunf Cave speleothem record from southern Oman (Fig. 9). In the Arabian Sea, there is a decline in the abundance of the cold water-loving foraminifera *Globigerina bulloides* between 5000 and 4000 cal years BP, suggesting decreased upwelling due to weaker monsoon winds, but this decline is not significantly greater than other periods of decline during the Holocene (Gupta et al., 2005). We find that several other paleo-monsoon records show a transition around 4200 years BP, the time of increased ENSO frequency in the El Junco record. In a review of Tibetan lake sediment records, Wei and Gasse (1999) note that five independent records demonstrate aridity and a weaker monsoon from 4500 to 3500 cal years BP. At least one other central Tibetan lake records also indicates a transition to higher aridity around 4200 cal years BP: there is a depositional hiatus in Ahung Co at 4000 cal years BP, indicating the lake dried out at this time of low monsoon precipitation (Morrill et al., 2006). An average of three speleothem $\delta^{18}O$ records from Dongge Cave, in the domain of both the SW and E Asian monsoons, also shows a decline in monsoon strength beginning around 4000 years BP (Fig. 9) (Yuan et al., 2004; Dykoski et al., 2005; Wang et al., 2005). Fleitmann et al. (2007) propose that the abrupt changes observed in lake sediment records during the Holocene are indicative of individual lake threshold responses to relatively minute changes in *P–E* values, rather than a significant, regional shift in monsoon intensity. This claim has merit for asynchronous changes in a network of lakes, but when a synchronous shift is recorded in multiple records, it suggests regional climatic variation rather than a series of individual lake thresholds.

Given the age model error in El Junco, and assuming equally large or larger error in many of the above records, we cannot be sure whether or not the decline in monsoon strength observed in some of the paleo-monsoon records preceded the hypothesized increase in ENSO frequency at 4200 cal years BP, or if they were both driven by some other forcing (internal or external to the climate system). Regardless, the similar timing of change in both the tropical Pacific and in the Asian monsoon region is suggestive of an interconnected system, and implies that a monsoon–ENSO linkage was present in the mid-Holocene.

The time period 2000–1000 years BP does not stand out as distinct in previous Asian monsoon syntheses. However, we find that a collection of high-resolution records, mostly from the SW Asian monsoon domain, show weak monsoon conditions between ~2500 and 1000 years BP. The decrease in the abundance of the cold water-loving foraminifera *Globigerina bulloides* in an ocean sediment core off the Oman Margin suggests the period of weakest Holocene upwelling and monsoon winds from 2400 to 1300 cal years BP (Gupta et al., 2005). The $\delta^{18}O$ speleothem record from Dongge Cave, China shows the highest Holocene $\delta^{18}O$ values, indicative of a weak monsoon, between 2500 and 1000 years BP (Yuan et al., 2004; Dykoski et al., 2005; Wang et al., 2005). A speleothem record from Hoti Cave in northern Oman indicates increased variance, with an abrupt shift to higher $\delta^{18}O$ values (weaker monsoon) between 2500 and 1000 years BP, while the southern Oman Qunf Cave speleothem record has a depositional hiatus, likely reflecting increased aridity and a weaker monsoon, from 2700 to 1400 years BP (Fleitmann et al., 2007). On the Tibetan Plateau, steppe vegetation replaces meadow vegetation from 2800 to 1600 cal years BP, indicating a weaker monsoon and more arid conditions (Shen et al., in press). Lake Qinghai and Selin Co, also on the Tibetan Plateau, reveal maximum Holocene aridity from 2300 to 1700 cal years BP (Wei and Gasse, 1999). Taking into account the age model uncertainty in the El Junco and monsoon records, it seems plausible that weaker monsoon variability likely preceded changes in the tropical Pacific at 2000 years BP, supporting the model-based inferences of Liu et al. (2000) and suggesting that the weak Asian monsoon may be related to anomalous ENSO variability at this time. We hypothesize that the ultimate cause of the anomalous ENSO and Asian monsoon behavior between 2000 and 1000 years BP may have been an orbitally induced reduction in mid-latitude insolation, but this hypothesis must await further examination. Moreover, the apparent lack of synchrony in some of the monsoon records from the SW and E Asian regions necessitates further inquiry into the mechanisms involved in a potential Holocene connection between the ENSO and Asian monsoon systems.

6. Conclusions

The synthesis of our new data from El Junco with previously published work brings ENSO variability over the Holocene into better focus. Records of grain size and C/N reveal a trend toward higher lake levels and wetter conditions at El Junco through the Holocene, with an abrupt, two-step transition to greater rainfall and higher lake levels at 3200 ± 160 and 2000 ± 80 cal years BP. Increased ENSO frequency began as early as 4200 ± 130 cal years BP, but there was also a period of increased ENSO frequency in the early Holocene between 9200 and 9000 cal years BP. The emerging consensus among several continuous proxies of ENSO variability constrains the initiation of stronger ENSO variability to ~4000 years BP, coincident with a decrease in the tropical Pacific SST gradient (Shulmeister and Lees, 1995; Rein et al., 2005; Koutavas et al., 2006). The period of greatest ENSO variance in the Holocene occurred between 2000 and 1500 cal years BP in the El Junco record and is confirmed as a time of greater ENSO activity by six independent ENSO reconstructions (Tudhope et al., 2001; Moy et al., 2002; Riedinger et al., 2002; Woodroffe et al., 2003; McGregor and Gagan, 2004; Rein et al., 2005).

The main driver of Galápagos climate change through the Holocene appears to be orbitally induced changes in seasonal insolation, which may have influenced the tropical Pacific directly through changes in the SST gradient, or indirectly via changes in the position of the ITCZ or the strength of the Asian Monsoon. However, the response to gradual insolation change is abrupt in El Junco, suggesting that nonlinear feedbacks in the climate system affect the response of the tropical Pacific to insolation changes. Anthropogenic greenhouse gas warming, rather than solar insolation, will likely influence future ENSO variability and climate change in the Galápagos archipelago in coming decades. Although paleoclimate records from the tropical Pacific and modeling simulations have now clarified the role of insolation in Holocene ENSO variability, additional high-resolution records are needed to reveal the full range of linkages between ENSO and other aspects of climate variability, such as the Asian monsoon and the ITCZ, particularly when it comes to understanding the patterns and mechanisms behind abrupt shifts in these important aspects of the climate system.

Acknowledgments

We are grateful for field assistance from M. Miller, J. Weiss, H. Barnett, T. Damassa, B. Fonseca, and R. Smittenberg. A. Cohen, P. Colinvaux, and J. Sachs are thanked for valuable discussion and helpful comments, W. Gosling for Galápagos climate data and M. Brenner and Z. Zhang for chronological data. Special thanks to the Galápagos National Park and the Charles Darwin Research Station for logistical support, The University of Arizona Department of Geosciences for additional funding, and The University of Arizona AMS Facility for radiocarbon dates. This research was also funded in part by a National Science Foundation Graduate Research Fellowship and NSF Grant ATM-0611320.

All data are available online at the World Data Center for Paleoclimatology (http://www.ncdc.noaa.gov/paleo/paleo.html).

References

An, Z.S., Porter, S.C., Kutzbach, J.E., Wu, X.H., Wang, S.M., Liu, X.D., Li, X.Q., Zhou, W.J., 2000. Asynchronous Holocene optimum of the East Asian monsoon. Quaternary Science Reviews 19 (8), 743–762.

Andrus, C.F.T., Crowe, D.E., Sandweiss, D.H., Reitz, E.J., Romanek, C.S., 2002. Otolith $\delta^{18}O$ record of mid-Holocene sea surface temperatures in Peru. Science 295 (5559), 1508–1511.

Appleby, P.G., 2001. Chronostratigraphic techniques in recent sediments. In: Last, W.M., Smol, J.P. (Eds.), Tracking Environmental Change Using Lake Sediments. Volume 1: Basin Analysis, Coring, and Chronological Techniques. Kluwer Academic Publishers, Dordrecht, pp. 171–203.

Appleby, P.G., Oldfield, F., 1978. The calculation of ^{210}Pb assuming a constant rate of supply of unsupported Pb-210 to the sediment. Catena 5, 1–8.

Appleby, P.G., Oldfield, F., 1983. The Assessment of ^{210}Pb data from sites with varying sediment accumulation rates. Hydrobiologia 103, 29–35.

Baker, C.B., Eischeid, J.K., Karl, T.R., Diaz, H.F., 1994. The quality control of long-term climatological data using objective data analysis. Preprints of AMS Ninth Conference on Applied Climatology, Dallas, TX.

Berger, A., Loutre, M.F., 1991. Insolation values for the climate of the last 10000000 years. Quaternary Science Reviews 10 (4), 297–317.

Carre, M., Bentaleb, I., Fontugne, M., Lavallee, D., 2005. Strong El Niño events during the early Holocene: stable isotope evidence from Peruvian sea shells. Holocene 15 (1), 42–47.

Chen, J.A., Wan, G.J., Zhang, D.D., Zhang, F., Huang, R.G., 2004. Environmental records of lacustrine sediments in different time scales: sediment grain size as an example. Science in China Series D 47 (10), 954–960.

Clement, A.C., Seager, R., Cane, M.A., 2000. Suppression of El Niño during the mid Holocene by changes in the Earth's orbit. Paleoceanography 15 (6), 731–737.

Cohen, A.S., 2003. Paleolimnology: The History and Evolution of Lake Systems. Oxford University Press, Oxford, New York, 500pp.

Cole, J.E., 2003. Holocene coral records: windows on tropical climate variability. In: McKay, A., Battarbee, R.W., Birks, H.J.B., Oldfield, F. (Eds.), Global Change in the Holocene. Arnold, London, pp. 437–452.

Colinvaux, P.A., 1968. Reconnaissance and chemistry of lakes and bogs of the Galápagos Islands. Nature 219 (5154), 590–594.

Colinvaux, P.A., 1969. Paleolimnological investigations in the Galápagos Archipelago. Mitteilungen Internationale Vereinigung fur Theoretische und Angewandte Limnologie 17, 126–130.

Colinvaux, P.A., 1972. Climate and Galápagos Islands. Nature 240 (5375), 17–20.

Colinvaux, P.A., 1984. The Galápagos climate: present and past. In: Perry, R. (Ed.), Key Environments: Galápagos. Pergamon Press, Oxford, pp. 55–69.

Colinvaux, P.A., Schofield, E.K., 1976a. Historical ecology in Galápagos Islands 1. A Holocene pollen record from El Junco Lake, Isla San Cristobal. Journal of Ecology 64 (3), 989–1012.

Colinvaux, P.A., Schofield, E.K., 1976b. Historical ecology in Galápagos Islands II. A Holocene spore record from El Junco Lake, Isla San Cristobal. Journal of Ecology 64 (3), 1013–1028.

Deser, C., Wallace, J.M., 1990. Large-scale atmospheric circulation features of warm and cold episodes in the tropical Pacific. Journal of Climate 3 (11), 1254–1281.

DeVries, T.J., Wells, L.E., 1990. Thermally-anomalous Holocene molluscan assemblages from coastal Peru-Evidence for paleogeographic, not climatic-change. Palaeogeography Palaeoclimatology Palaeoecology 81 (1/2), 11–32.

DeVries, T.J., Ortlieb, L., Diaz, A., Wells, L., Hillaire-Marcel, C., 1997. Determining the early history of El Niño. Science 276 (5314), 965–966.

Dykoski, C.A., Edwards, R.L., Cheng, H., Yuan, D.X., Cai, Y.J., Zhang, M.L., Lin, Y.S., Qing, J.M., An, Z.S., Revenaugh, J., 2005. A high-resolution, absolute-dated Holocene and deglacial Asian monsoon record from Dongge Cave, China. Earth and Planetary Science Letters 233 (1/2), 71–86.

Fleitmann, D., Burns, S.J., Mudelsee, M., Neff, U., Kramers, J., Mangini, A., Matter, A., 2003. Holocene forcing of the Indian monsoon recorded in a stalagmite from Southern Oman. Science 300 (5626), 1737–1739.

Fleitmann, D., Burns, S.J., Mangini, A., Mudelsee, M., Kramers, J., Villa, I., Neff, U., Al-Subbary, A.A., Buettner, A., Hippler, D., Matter, A., 2007. Holocene ITCZ and Indian monsoon dynamics recorded in stalagmites from Oman and Yemen (Socotra). Quaternary Science Reviews 26 (1/2), 170–188.

Flower, R.J., 1993. Diatom preservation—experiments and observations on dissolution and breakage in modern and fossil material. Hydrobiologia 269, 473–484.

Fontugne, M., Usselmann, P., Lavallee, D., Julien, M., Hatte, C., 1999. El Niño variability in the coastal desert of southern Peru during the mid-Holocene. Quaternary Research 52 (2), 171–179.

Gagan, M.K., Ayliffe, L.K., Hopley, D., Cali, J.A., Mortimer, G.E., Chappell, J., McCulloch, M.T., Head, M.J., 1998. Temperature and surface–ocean water balance of the mid-Holocene tropical Western Pacific. Science 279 (5353), 1014–1018.

Gupta, A.K., Das, M., Anderson, D.M., 2005. Solar influence on the Indian summer monsoon during the Holocene. Geophysical Research Letters 32(17), L17703 doi:10.1029/2005GL022685.

Haug, G.H., Hughen, K.A., Sigman, D.M., Peterson, L.C., Rohl, U., 2001. Southward migration of the intertropical convergence zone through the Holocene. Science 293 (5533), 1304–1308.

He, Y., Theakstone, W.H., Zhang, Z.L., Zhang, D.A., Yao, T.D., Chen, T., Shen, Y.P., Pang, H.X., 2004. Asynchronous Holocene climatic change across China. Quaternary Research 61 (1), 52–63.

Hedges, R.E.M., Law, I.A., Bronk, C.R., Housley, R.A., 1989. The Oxford Accelerator Mass-Spectrometry Facility—technical developments in routine dating. Archaeometry 31, 99–113.

Kitoh, A., Murakami, S., 2002. Tropical Pacific climate at the mid-Holocene and the Last Glacial Maximum simulated by a coupled ocean–atmosphere general circulation model. Paleoceanography 17 (3), 1047.

Koutavas, A., Lynch-Stieglitz, J., Marchitto, T.M., Sachs, J.P., 2002. El Niño-like pattern in ice age tropical Pacific sea surface temperature. Science 297 (5579), 226–230.

Koutavas, A., DeMenocal, P.B., Olive, G.C., Lynch-Stieglitz, J., 2006. Mid-Holocene El Niño-Southern Oscillation (ENSO) attenuation revealed by individual foraminifera in eastern tropical Pacific sediments. Geology 34 (12), 993–996.

Krishnaswamy, S., Lal, D., Martin, J.M., Meybeck, M., 1971. Geochronology of lake sediments. Earth and Planetary Science Letters 11 (5), 407–414.

Kumar, K.K., Rajagopalan, B., Cane, M.A., 1999. On the weakening relationship between the Indian monsoon and ENSO. Science 284 (5423), 2156–2159.

Latorre, O.T., 1999. El Hombre en las Islas Encantadas, Quito, 446pp.

Lea, D.W., Pak, D.K., Belanger, C.L., Spero, H.J., Hall, M.A., Shackleton, N.J., 2006. Paleoclimate history of Galápagos surface waters over the last 135,000 yr. Quaternary Science Reviews 25 (11/12), 1152–1167.

Liu, Z.Y., Kutzbach, J., Wu, L.X., 2000. Modeling climate shift of El Niño variability in the Holocene. Geophysical Research Letters 27 (15), 2265–2268.

Liu, Z.Y., Harrison, S.P., Kutzbach, J., Otto-Bliesner, B., 2004. Global monsoons in the mid-Holocene and oceanic feedback. Climatic Dynamics 22 (2/3), 157–182.

Loubere, P., Richaud, M., Liu, Z.Y., Mekik, F., 2003. Oceanic conditions in the eastern equatorial Pacific during the onset of ENSO in the Holocene. Quaternary Research 60 (2), 142–148.

McCormac, F.G., Hogg, A.G., Blackwell, P.G., Buck, C.E., Higham, T.F.G., Reimer, P.J., 2004. SHCal04 Southern Hemisphere calibration, 0–11.0 cal kyr BP. Radiocarbon 46 (3), 1087–1092.

McCulloch, M., Mortimer, G., Esat, T., Li, X.H., Pillans, B., Chappell, J., 1996. High-resolution windows into early Holocene climate: Sr/Ca coral records from the Huon Peninsula. Earth and Planetary Science Letters 138 (1/4), 169–178.

McGregor, H.V., Gagan, M.K., 2004. Western Pacific coral $\delta^{18}O$ records of anomalous Holocene variability in the El Niño-Southern Oscillation Geophysical Research Letters 31(11), L11204, doi:10.1029/2004GL019972.

McMullen, C.K., 1999. Flowering Plants of the Galápagos. Cornell University, Ithaca, 370pp.

Meyers, P.A., 1994. Preservation of elemental and isotopic source identification of sedimentary organic-matter. Chemical Geology 114 (3/4), 289–302.

Meyers, P.A., Ishiwatari, R., 1993. Lacustrine organic geochemistry—an overview of indicators of organic-matter sources and diagenesis in lake-sediments. Organic Geochemistry 20 (7), 867–900.

Mitchell, T.P., Wallace, J.M., 1992. The annual cycle in equatorial convection and sea-surface temperature. Journal of Climate 5 (10), 1140–1156.

Morrill, C., Overpeck, J.T., Cole, J.E., 2003. A synthesis of abrupt changes in the Asian summer monsoon since the last deglaciation. Holocene 13 (4), 465–476.

Morrill, C., Overpeck, J.T., Cole, J.E., Liu, K.B., Shen, C.M., Tang, L.Y., 2006. Holocene variations in the Asian monsoon inferred from the geochemistry of lake sediments in central Tibet. Quaternary Research 65 (2), 232–243.

Moy, C.M., Seltzer, G.O., Rodbell, D.T., Anderson, D.M., 2002. Variability of El Niño/Southern Oscillation activity at millennial timescales during the Holocene epoch. Nature 420 (6912), 162–165.

Nesje, A., 1992. A piston corer for lacustine and marine sediments. Arctic and Alpine Research 24 (3), 257–259.

Otto-Bliesner, B.L., Brady, E.C., Shin, S.I., Liu, Z.Y., Shields, C., 2003. Modeling El Niño and its tropical teleconnections during the last glacial–interglacial cycle. Geophysical Research Letters 30(23), 2198, doi:10.1029/2003GL018553.

Palacios, D.M., 2004. Seasonal patterns of sea-surface temperature and ocean color around the Galápagos: regional and local influences. Deep-Sea Research II 51 (1–3), 43–57.

Penman, H.L., 1948. Natural evaporation from open water, bare soil and grass. Proceedings of the Royal Society of London Series-A 193 (1032), 120–145.

Reimer, P.J., Brown, T.A., Reimer, C.W., 2004. Discussion: reporting and calibration of post-bomb ^{14}C data. Radiocarbon 46 (3), 1299–1304.
Rein, B., Luckge, A., Reinhardt, L., Sirocko, F., Wolf, A., Dullo, W.C., 2005. El Niño variability off Peru during the last 20,000 years. Paleoceanography 20 (4), 2004PA001099.
Riedinger, M.A., Steinitz-Kannan, M., Last, W.M., Brenner, M., 2002. A ~6100 ^{14}C yr record of El Niño activity from the Galápagos Islands. Journal of Paleolimnology 27 (1), 1–7.
Rodbell, D.T., Seltzer, G.O., Anderson, D.M., Abbott, M.B., Enfield, D.B., Newman, J.H., 1999. A ~15,000-year record of El Niño-driven alluviation in southwestern Ecuador. Science 283 (5410), 516–520.
Rossow, W.B., Walker, A.W., Beuschel, D.E., Roiter, M.D., 1996. International Satellite Cloud Climatology Project (ISCCP) Documentation of New Cloud Datasets. WMO/TD-No. 737, World Meteorological Organization.
Sandweiss, D.H., Maasch, K.A., Burger, R.L., Richardson, J.B., Rollins, H.B., Clement, A., 2001. Variation in Holocene El Niño frequencies: climate records and cultural consequences in ancient Peru. Geology 29 (7), 603–606.
Schnurrenberger, D., Russell, J., Kelts, K., 2003. Classification of lacustrine sediments based on sedimentary components. Journal of Paleolimnology 29 (2), 141–154.
Shanahan, T.M., Overpeck, J.T., Sharp, W.E., Scholz, C.A., Arko, J.A., 2007. Simulating the response of a closed-basin lake to recent climate and land-use changes in tropical West Africa (Lake Bosumtwi, Ghana). Hydrological Processes 21 (13), 1678–1691.
Shen, C., Liu, K.B., Morrill, C., Overpeck, J.T., Peng, J., Tang, L. Meadow–steppe ecotone shift and major centennial-scale droughts during the mid-late Holocene in the central Tibetan Plateau. Ecology, in press.
Shulmeister, J., Lees, B.G., 1995. Pollen evidence from Tropical Australia for the onset of an ENSO-dominated climate at C 4000 BP. Holocene 5 (1), 10–18.
Shuttleworth, W.J., 1993. Evaporation. In: Maidment, D.R. (Ed.), Handbook of Hydrology. McGraw-Hill, pp. 4.1–4.53.
Smith, T.M., Reynolds, R.W., 2004. Improved extended reconstruction of SST (1854–1997). Journal of Climate 17, 2466–2477.
Snell, H., Rea, S., 1999. The 1997-98 El Niño in the Galápagos: can 34 years of data estimate 120 years of pattern? Noticias de Galápagos 60, 11–20.
Steinitz-Kannan, M., Riedinger, M.A., Last, W.M., Brenner, M., Miller, M.C., 1998. Un registro de 6,000 años de manifestaciones intensas del fenomeno de El Niño en sedimentos de lagunas de las Islas Galápagos. Bulletin de l'Institute Français d'études Andines 27 (3), 581–592.
Stott, L., Cannariato, K., Thunell, R., Haug, G.H., Koutavas, A., Lund, S., 2004. Decline of surface temperature and salinity in the western tropical Pacific Ocean in the Holocene epoch. Nature 431 (7004), 56–59.
Stuiver, M., Reimer, P.J., 1993. Extended ^{14}C data-base and revised calib 3.0 ^{14}C age calibration program. Radiocarbon 35 (1), 215–230.
Sun, D.H., Bloemendal, J., Rea, D.K., Vandenberghe, J., Jiang, F.C., An, Z.S., Su, R.X., 2002. Grain-size distribution function of polymodal sediments in hydraulic and aeolian environments, and numerical partitioning of the sedimentary components. Sedimentary Geology 152 (3/4), 263–277.
Tudhope, A.W., Chilcott, C.P., McCulloch, M.T., Cook, E.R., Chappell, J., Ellam, R.M., Lea, D.W., Lough, J.M., Shimmield, G.B., 2001. Variability in the El Niño-Southern oscillation through a glacial–interglacial cycle. Science 291 (5508), 1511–1517.
Verardo, D.J., Froelich, P.N., Mcintyre, A., 1990. Determination of organic-carbon and nitrogen in marine-sediments using the Carlo-Erba-Na-1500 analyzer. Deep-Sea Research 37 (1), 157–165.
Wang, Y.J., Cheng, H., Edwards, R.L., He, Y.Q., Kong, X.G., An, Z.S., Wu, J.Y., Kelly, M.J., Dykoski, C.A., Li, X.D., 2005. The Holocene Asian monsoon: links to solar changes and North Atlantic climate. Science 308 (5723), 854–857.
Webster, P.J., Magana, V.O., Palmer, T.N., Shukla, J., Tomas, R.A., Yanai, M., Yasunari, T., 1998. Monsoons: processes, predictability, and the prospects for prediction. Journal of Geophysical Research—Oceans 103 (C7), 14451–14510.
Wei, K., Gasse, F., 1999. Oxygen isotopes in lacustrine carbonates of West China revisited: implications for post glacial changes in summer monsoon circulation. Quaternary Science Reviews 18 (12), 1315–1334.
Wiggins, I.L., Porter, D.M., 1971. Flora of the Galápagos Islands. Stanford University Press, Stanford, 998pp.
Wolter, K., Timlin, M.S., 1998. Measuring the strength of ENSO events-How does 1997/98 rank? Weather 53, 315–324.
Woodroffe, C.D., Beech, M.R., Gagan, M.K., 2003. Mid-late Holocene El Niño variability in the equatorial Pacific from coral microatolls. Geophysical Research Letters, 30(7), 1358, doi:10.1029/2002GL015868.
Yuan, D.X., Cheng, H., Edwards, R.L., Dykoski, C.A., Kelly, M.J., Zhang, M.L., Qing, J.M., Lin, Y.S., Wang, Y.J., Wu, J.Y., Dorale, J.A., An, Z.S., Cai, Y.J., 2004. Timing, duration, and transitions of the Last Interglacial Asian Monsoon. Science 304 (5670), 575–578.
Zebiak, S.E., Cane, M.A., 1987. A model El-Niño Southern Oscillation. Monthly Weather Review 115 (10), 2262–2278.